

https://doi.org/10.1070/QEL16061

Measurement and correction of the wavefront of the laser light in a turbid medium

I.V. Galaktionov, A.V. Kudryashov, Yu.V. Sheldakova, A.A. Byalko, G. Borsoni

We report a numerical and experimental study of the laser beam propagation through a suspension of polystyrene microspheres in distilled water, showing the presence of higher-order centrally symmetric aberrations for the scatterer concentrations in the range from 1.3×10^5 to 10^6 mm^{-3} and analysing the dependence of the scattered light wavefront distortion on the concentration of particles in a turbid medium. The study has also shown the effectiveness of the compensation of the wavefront aberrations of a scattered laser beam using a bimorph adaptive mirror.

Keywords: *turbid medium, light scattering, Shack–Hartmann wavefront sensor, wavefront corrector, adaptive optics.*

1. Introduction

A medium is considered turbid or scattering if it has a pronounced optical inhomogeneity due to the presence of impurities of particles with a different refractive index. A striking example is the atmospheric aerosol, haze, fog and biological tissue [1]. In such media, part of the beam energy is absorbed, while some of the energy is redistributed in space, forming a halo of the scattered light, which makes the contours of these objects blurred and prevents radiation focusing. Solving this problem is of particular significance for applications aimed at increasing the distance travelled by the light, pattern recognition, information transmission by optical communication channels, as well as for medical noninvasive diagnosis, in particular for the study of the state of blood vessels and retina and diagnosis of malignant and benign tumours [2–4].

The study of the propagation of light through a randomly inhomogeneous medium relies on different approaches, the essence of which is to find the solution of the transport equation: the method of path integrals, methods of diffusion approximation, method of the light scattering by Brownian particles and method of small-angle approximation [5]. However, all these approaches are not universal because they are based on the theoretical results obtained under different assumptions. Therefore, use is often made of the stochastic Monte Carlo simulation, which gives an approximate solution to the transport equation for any conditions of the problem: arbitrary configurations of the medium and boundary conditions. The Monte Carlo method involves modelling the behaviour of individual elementary parts of a physical system; in particular, for the problem of propagation of light it takes into account the quantum nature of light and simulates the behaviour of the photon flux [6].

Traditionally, the scattered light consists of photons of three types [7]: ballistic, on-axis (or snake photons) and off-axis (or diffusive photons). Ballistic photons travel through a turbid medium in straight line paths and do not interact with the scatterers. This coherent component of the scattered light is the best for imaging. On-axis photons, having undergone few scattering events with the scatterers, travel in near-forward paths along a trajectory that is close to the initial direction of the beam propagation. These photons are beginning to play an important role when the scattering medium layer thickness increases, because the number of ballistic photons in this case decreases exponentially [2]. Off-axis photons experience multiple scattering in all directions and form a noncoherent component of the scattered light.

As noted above, ballistic photons are responsible for the formation of an undistorted image of the object, but their number decreases exponentially with increasing layer thickness or concentration of the turbid medium. Therefore, it is necessary to take into account the effect of snake and diffusive photons on the distribution of intensity and phase of the scattered light. To increase the efficiency of distinguishing malignant tumours from benign tumours, Zhang et al. [8] have successfully applied the combined spectral analysis method [8]. Contrast enhancement of images of these objects has become possible through the use of the principles of holography based on the reversibility of the scattering process [9, 10]. Matthews et al. [11] describe a method of multispectral multiple scattering low coherence interferometry using the principles of coherence and spatial filtering to produce millimetre-resolution images of objects located in a biological tissue at a depth down to 9 mm. Zhou et al. [12] introduce a new all-optical method of time-reversed focusing on moving targets through scattering samples, which they termed 'time reversal by analysis of changing wavefronts from kinetic targets'. Bertolotti et al. [13] suggest using a non-invasive method to retrieve the shape of fluorescent objects hidden behind a scattering layer. For the problems of focusing [14] and restoration of images of objects located inside or outside a layer of a scattering medium [15–19], Vellekoop et al. [14] have used phase modulators.

In this paper, we present numerical and experimental measurements of the wavefront of the laser light transmitted through a turbid medium, by using a Shack–Hartmann sensor. We have also demonstrated the possibility of compensa-

I.V. Galaktionov, A.V. Kudryashov, Yu.V. Sheldakova, A.A. Byalko
Active optics NightN Ltd., ul. Sudostroitel'naya 18, Bld. 5, 115407 Moscow, Russia; e-mail: galaktionov@activeoptics.ru;
G. Borsoni AKA Optics SAS, Hotel Technoptic, 2 rue Marc Donadille, CS80001, 13453 Marseille Cedex 13, France

Received 29 February 2016; revision received 25 October 2016
Kvantovaya Elektronika **47** (1) 32–37 (2017)
Translated by I.A. Ulitkin

tion of the measured distortions by a bimorph adaptive mirror [20]. To calculate the intensity and phase of the scattered light, we have implemented a computer Monte-Carlo-based model of the light propagation in a turbid medium. The programme provides an opportunity for the formation of hartmannograms (images of the focal spot of a microlens array of the Shack–Hartmann sensor). We have developed an experimental setup for measuring aberrations of the laser light transmitted through a cuvette with a suspension of polystyrene microspheres in distilled water. To compensate for the measured aberrations we have used experimentally measured response functions of the bimorph mirror with 32 electrodes.

2. Model of the light propagation in a turbid medium

2.1. Monte Carlo method

In the present study, we have investigated the scattering of the laser light with a wavelength $\lambda = 0.65$ μm [21] by 1 μm-diameter polystyrene microspheres suspended in distilled water. The particle concentration was varied from 1.3×10^5 to 10^6 mm^{-3}. The initial beam aperture was 4 mm, the refractive index of the medium was equal to 1.33, and the refractive index of polystyrene microspheres for the selected wavelength amounted to 1.582 [22].

To simulate the propagation of the light through a scattering medium we used the stochastic Monte Carlo method [23]. Its essence consists in multiple realisations of a random process, the probability characteristics of which coincide with the physical quantities used in the problem [24]. The laser beam at a particular point in time is represented in the form of a large number of photons (in the present study, 2.5×10^{11}) evenly distributed over the initial aperture, which is physically equivalent to the uniform distribution of the beam intensity (Fig. 1).

The paper considers a collimated beam of the light; therefore, the initial direction of all the photons was all the same (perpendicular to the layer of a turbid medium). The distance between two successive collisions of a photon with scatterers, called the mean free path, was calculated by the formula $l = -\ln\xi_l/\mu_s$, where μ_s is the scattering coefficient of a medium [24], and ξ_l is a random number uniformly distributed on the interval [0, 1). The scattering coefficient μ_s is measured in inverse millimetres and is one of the main characteristics of a turbid medium: it shows the strength of the scattering per unit length. This coefficient is calculated by the formulas of Mie theory [24]. As a phase function, in modelling the scattering angle as a function of parameters of the scattering medium we used the Henyey–Greenstein function due to the high speed of its calculation and to the fact that it accurately approximates the function of the light scattering at selected concentrations [25]. To determine a new propagation direction of a photon after its collision with a scatterer, we calculated two angles. The angle between the current and new directions of motion (called the scattering angle θ) and the angle between the projection of the new direction of motion to a plane perpendicular to the initial direction and some fixed axis on this plane (called the azimuthal angle φ) were calculated as follows [24]:

$$\cos\theta = \begin{cases} \frac{1}{2g}\left[1 + g^2 - \left(\frac{1-g^2}{1-g+2g\xi_\theta}\right)^2\right], g > 0, \\ 2\xi_\theta - 1, g = 0, \end{cases}, \quad (1)$$

$$\varphi = 2\pi\xi_\varphi. \quad (2)$$

Here, g is the anisotropy factor [24]; and ξ_θ and ξ_φ are random quantities uniformly distributed on the interval [0, 1). Based on the mean free path and the new direction of motion, we calculated a new position of a photon in space and checked if the medium boundaries cross. If the photon stayed within the scattering volume, calculations of l, θ and φ were repeated. Thus, at the end of the modelling process, we had information about the optical length of the traversed path and the final direction of the propagation of each photon.

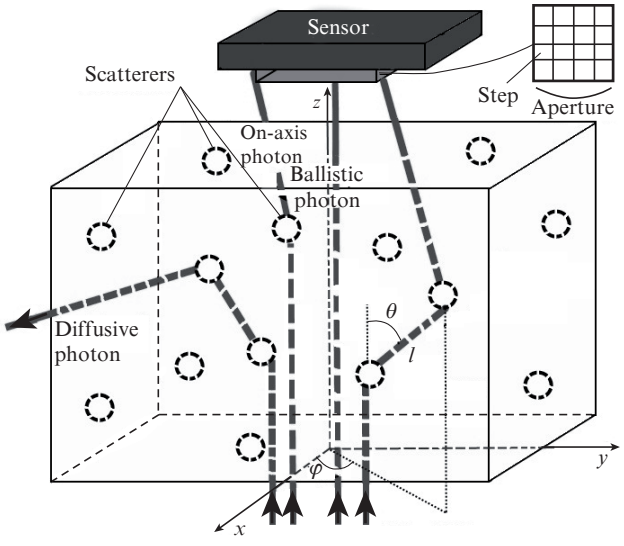

Figure 1. Scheme of photon scattering on inhomogeneities of a turbid medium.

2.2. Model of the Shack–Hartmann sensor for wavefront measurements

For wavefront aberrations of the light transmitted through a turbid medium layer to be numerically measured, we developed a Shack–Hartmann sensor model implementing a simplified real sensor: an array of microlenses with a diameter of 150 μm and a focal length $f = 6$ mm, and a CCD-camera sensor located in the focal plane of the lenslet array.

Let us consider the movement of a photon passing through a turbid medium and incident on one of the sub-apertures of the lenslet array. We introduce a local Cartesian coordinate system with a centre corresponding to the centre of the array sub-aperture. Suppose that a photon incident on the lens has some random direction defined by the direction cosines μ_x, μ_y and μ_z along the axes x, y and z, respectively. Then, its position on the sensor after passing through the lens can be calculated by the formulas $x_f = f\mu_x/\mu_z$, $y_f = f\mu_y/\mu_z$, $z_f = f$. After performing the same calculations for all photons, we obtained images of the focal spots on the sensor, i.e. a hartmannogram.

To assess the aberrations of the light we should have a reference wavefront. For a hartmannogram of this wavefront to be retrieved, a collimated laser beam propagated from the source to the sensor in the absence of a scattering medium. Photons incident on the microlens array were concentrated,

in this case, in their foci on the sensor. Thus, a hartmannogram of the reference wavefront was formed. In the presence of a turbid medium in the beam path, on-axis and diffusive photons fell on the microlens array at nonzero angles with respect to their initial direction, parallel to the optical axis of the system. As a result, in the plane of the CCD-camera sensor there emerged focal spots of some diameter with the centres, the positions of which, generally speaking, were different from the positions of the centres of the reference beam focal spots.

To estimate the aberrations, the Shack–Hartmann wavefront sensor used an algorithm based on the calculation of the shifts of the focal spot centres. The positions of the focal spot centres were calculated as the positions of the centres of gravity [26]. Based on the magnitude of the shifts of the focal spots, we calculated the local tilts of the wavefront. The phase surface was approximated by Zernike polynomials [27]. The results of numerical experiments showed the tendency to an increase in centrally symmetric aberrations with increasing concentration of scatterers (Table 1).

Table 1. Terms of Zernike polynomials, PV and RMS of the wavefront for different concentrations of scatterers in a turbid medium.

Concentration/10^5 mm^{-3}	PV/λ	RMS/λ	Defocusing/λ ($2\rho^2-1$)	Spherical aberration/λ ($6\rho^4-6\rho^2+1$)
1.3	2.64	0.59	0.74	0.82
7.38	2.78	0.62	0.91	0.86
9.43	3.28	0.76	1.02	1.03
10.2	3.57	0.83	1.12	1.11

Notes: PV is the peak-to-valley wavefront aberrations; RMS is the root-mean-square deviation; ρ is the modulus of the radius vector in the beam cross section.

Figure 2 shows the interferogram of the wavefront of the laser beam transmitted through a turbid medium with a particle concentration of 7.4×10^5 mm^{-3}, and the corresponding terms of some Zernike polynomials are presented in Table 2.

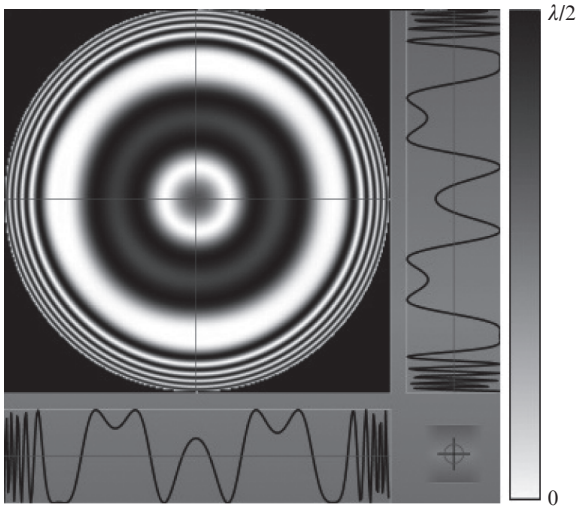

Figure 2. Interferogram of the wavefront of a beam transmitted through a turbid medium with a scatterer concentration of 7.4×10^5 mm^{-3}.

Table 2. Terms of Zernike corresponding to the interferogram shown in Fig. 2.

Polynomial No.	Aberration	Term/λ
1	Tilt along the x axis ($\rho\cos\theta$)	0.008
2	Tilt along the y axis ($\rho\sin\theta$)	0.005
3	Defocusing ($2\rho^2-1$)	0.798
…	…	…
8	Spherical aberration ($6\rho^4-6\rho^2+1$)	0.866
…	…	…
15	Spherical aberration ($20\rho^6-30\rho^4+12\rho^2-1$)	0.559
…	…	…
24	Spherical aberration ($70\rho^8-140\rho^6+90\rho^4-20\rho^2+1$)	−0.166

3. Experimental measurements of the wavefront

3.1. Experimental setup

For measuring the distortion of the laser beam in a turbid medium we assembled an experimental setup whose scheme is shown in Fig. 3. The laser beam passed through a glass cuvette with a suspension of 1 μm-diameter polystyrene microspheres in distilled water and was incident on the Shack–Hartmann wavefront sensor [28–31]. The sensor consisted of a digital Basler A302fs CCD camera equipped with a 1/2-inch sensor (the size of the receiving area of the sensor is 6.4 × 4.8 mm) and of a lenslet array (focal length, 6 mm; distance between microlens, 150 μm; number of microlenses is greater than 1350). The camera frame rate was 30 Hz.

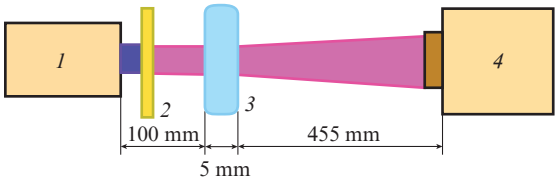

Figure 3. Schematic of the experimental setup: (*1*) diode laser with a wavelength of 0.65 μm and an output aperture of 4 mm; (*2*) optical filter; (*3*) glass cuvette with a turbid medium; (*4*) Shack–Hartmann wavefront sensor.

3.2. Measurement results

The wavefront was analysed in the 4.8 mm-diameter aperture, the centre of which coincides with the centre of the camera's sensor [32]. Increasing the aperture diameter relative to the initial beam size was due to the need to analyse the contribution of the on-axis and diffusive photons into the light wavefront. The phase surface measured by the Shack–Hartmann sensor was approximated by Zernike polynomials. Dependences of the wavefront aberrations expressed in terms of symmetric Zernike polynomials Nos 3, 8 and 15 [33] on the concentration of polystyrene microspheres are shown in Fig. 4. The wavefront measurements by the Shack–Hartmann sensor were carried out by averaging over 10 frames coming from this sensor with a frequency of 30 Hz. One can see that defocusing (the term of Zernike polynomial No. 3 increased

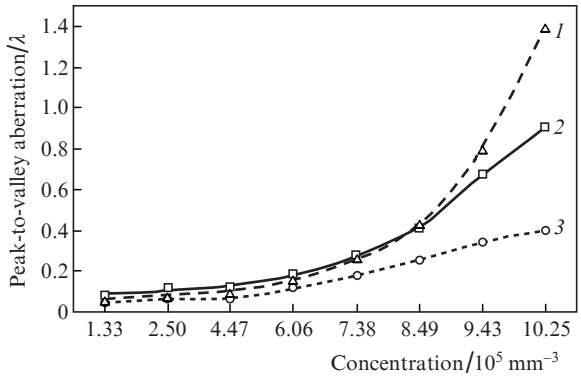

Figure 4. Peak-to-valley wavefront aberrations as functions of concentration of scatterers in a turbid medium in the case of (*1*) defocusing (Zernike polynomial No. 3) and spherical aberrations of (*2*) lower (Zernike polynomial No. 8) and (*3*) higher (Zernike polynomial No. 15) orders.

from 0.12λ to 1.39λ) and spherical aberration (the term of Zernike polynomial No. 8 increased from 0.09λ to 0.91λ) significantly increased with increasing particle concentration.

As an example, consider the wavefront of the light transmitted through a turbid medium with a scatterer concentration of 7.4×10^5 mm^{-3}. The interferogram of this wavefront is shown in Fig. 5c. The root-mean-square (RMS) deviation of the surface, calculated from the first 24 Zernike polynomials (RMS_{24}), is in this case equal to 0.217λ. If only lower order aberrations are taken into account (the terms of Zernike polynomials Nos 3–8), and all other terms are artificially zeroed, the rms deviation RMS_8 is equal to 0.192λ. Similar results hold for other values of the concentrations used in this study (Table 3).

3.3. Wavefront measurement problems

Due to the symmetrical nature of Mie scattering, we expected to see only centrally symmetric aberrations in the measurement of the wavefront of the scattered light, such as defocusing and spherical aberration (Fig. 5b). However, the studies conducted have demonstrated the presence of a range of lower- and higher-order aberrations. Possible reasons for this are as follows:

Table 3. RMS deviations of the wavefront approximated by the first 24 Zernike polynomials (RMS_{24}) and the first 8 Zernike polynomials (RMS_8).

Concentration/10^5 mm^{-3}	RMS_{24}/λ	RMS_8/λ
1.3	0.077	0.058
2.5	0.085	0.077
4.5	0.103	0.095
6.0	0.155	0.138
7.4	0.217	0.192
8.5	0.377	0.349
9.4	0.611	0.588
10.3	0.958	0.945

1. Nonideal surfaces of the walls of the glass cuvette used.
2. The presence of turbulent fluctuations in the medium in the path of the light beam.

The measurements by the Shack–Hartmann sensor showed that the glass cuvette had non-parallel walls, which led to the emergence of the wavefront tilt. The peak-to-valley (PV) wavefront aberration of the laser beam transmitted through an empty cuvette (Fig. 5a) was 1.05 μm (1.62λ), the rms deviation was found to be 0.3 μm (0.46λ), the slope along the x axis was −0.6 μm (-0.9λ), and the magnitude of the coma along the x axis was equal to −0.05 μm (-0.08λ). By filling the cuvette with a suspension of scattering particles, the coma also increased as a result of the displacement of the beam from the optical axis of the system.

4. Wavefront correction

4.1. Bimorph deformable mirror

Table 3 shows that the main contribution to the distortion of the scattered light wavefront is made by centrally symmetric, lower-order aberrations. To compensate for such distortions, use is traditionally made of a bimorph deformable mirror [34, 35]. A bimorph mirror is composed of two glued plates: a relatively thick (about 2 mm) glass or metal substrate (the thickness depends on the mirror diameter) with a reflective coating and a thin (0.3 mm) piezoceramic substrate (Fig. 6a). Both sides of the piezoceramic disk (piezodisk) have electrodes. When a voltage is applied to an electrode, due to the reverse piezoelectric effect the piezodisk either expands or

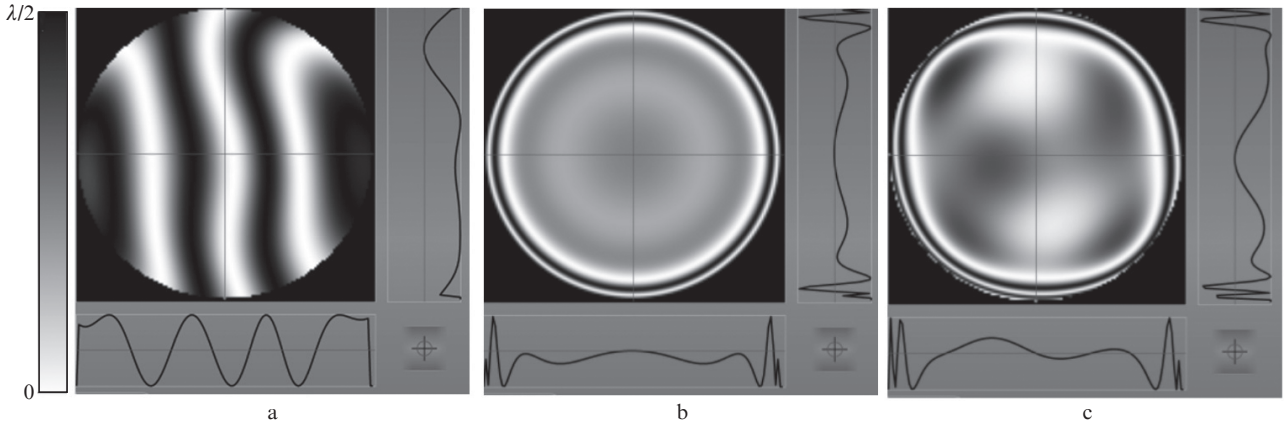

Figure 5. (a) Aberrations introduced by a glass cuvette, (b) expected interferogram of the wavefront of the light transmitted through a turbid medium at a scatterer concentration of 7.4×10^5 mm^{-3} and (c) interferogram of the actually measured wavefront.

contracts (depending on the sign of the voltage) in the radial direction. This leads to a bending of the glued substrate with a reflective coating. To reproduce different types of aberrations with the help of such a corrector, the outer electrode is divided into a large number of separate sectors. An example of a grid of electrodes is shown in Fig. 6b. The size and number of electrodes depends on the type of aberrations to be compensated for. Sometimes it is useful to use an additional piezodisk with a bulk electrode for reproducing defocusing.

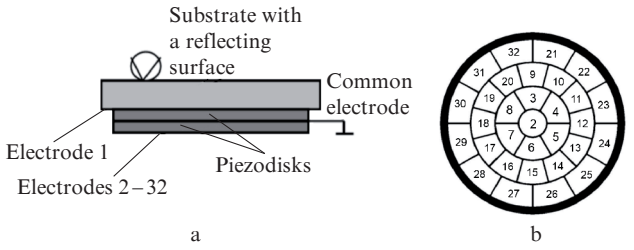

Figure 6. (a) Schematic of a bimorph mirror with 32 electrodes and (b) arrangement of these electrodes.

A feature of adaptive bimorph mirrors is that they can effectively reproduce lower-order aberrations. This is very important in our case because, as mentioned above, defocusing and lower-order spherical aberration make the largest contribution to the distortion of the scattered light wavefront. Figure 7 shows the interferograms of the wavefronts corresponding to Zernike polynomials Nos 3 and 8, reproduced using a bimorph adaptive mirror with 32 electrodes. The amplitudes of the initial phase surface that was necessary to reproduce were 2 μm (polynomial No. 3) and 1.2 μm (polynomial No. 8). A residual error of reproduction, i.e. the rms deviation of the phase surface calculated as the point-to-point difference between the amplitudes of the restored and initial surfaces, was 0.03 μm for defocusing and 0.005 μm for spherical aberration. This suggests a high accuracy of reproduction of given symmetric Zernike polynomials by a bimorph deformable mirror.

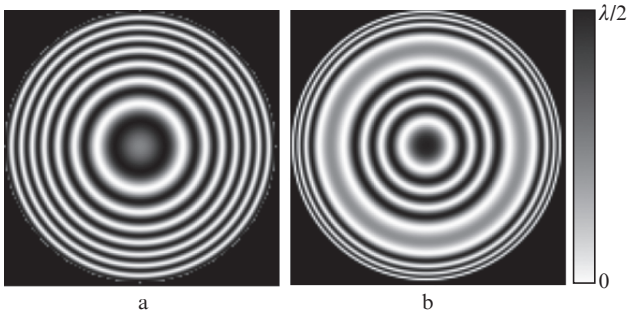

Figure 7. Interferograms of Zernike polynomials (a) No. 3 and (b) No. 8 reproduced by a bimorph adaptive mirror with 32 electrodes.

4.2. Correction algorithm

The experimentally measured phase surface of the light transmitted through a turbid medium was approximated by the response functions of mirror electrodes. The response function of an electrode is a set of displacement coordinates of the focal spots in response to the voltage with unit amplitude applied to the given electrode. The required voltages on the electrodes of the deformable mirror were calculated in such a way that the coordinates of the analysed beam focal spot centres after applying corrective voltages maximally coincided with the coordinates of the reference beam focal spot centres. The matrix of shifts of the focal spot centres is given by the expression

$$S_k = \left| \begin{matrix} \Delta x_k \\ \Delta y_k \end{matrix} \right| = \sum_{j=1}^{N} u_j b_j(x_k, y_k),$$

where Δx_k is the displacement of the kth focal spot along the x axis; Δy_k is the displacement of the kth focal spot along the y axis; N is the number of mirror electrodes; u_j is the voltage on the jth electrode; and $b_j(x_k, y_k)$ is the response function of the jth electrode at point (x_k, y_k).

After calculating the displacement of the focal spots and measuring the response functions of the adaptive mirror we calculated the voltages applied to the electrodes by the method of least squares [27]. Applying a voltage to the mirror electrodes caused a bending of the reflecting surface, which, in turn, led to the displacement of the focal spots detected by the Shack–Hartmann sensor [36]. On the basis of new data on the position of the focal spots we calculated a new set of voltages. This procedure was repeated until the minimum required difference in amplitudes of the reference and corrected wavefronts was achieved.

4.3. Results of correction

Table 4 presents peak-to-valley wavefront aberrations for each concentration in question before and after correction using the response functions of the bimorph mirror. For example, it is clear that for a concentration of 7.4×10^5 mm^{-3} the peak-to-valley aberrations were reduced from 1.26λ to 0.05λ .

Table 4. Peak-to-valley wavefront aberrations of the light transmitted through a layer of a scattering medium with different concentrations.

Concentration/10^5 mm^{-3}	PV before correction/λ	PV after correction/λ
1.3	0.46	0.05
2.5	0.51	0.05
4.5	0.66	0.05
6.0	1.06	0.05
7.4	1.26	0.05
8.5	2.34	0.03
9.4	3.29	0.03
10.3	4.23	0.06

Figure 8 shows the interferograms of the wavefront of the light transmitted through a turbid medium with a scattering particle concentration of 7.4×10^5 mm^{-3} before and after correction by the bimorph mirror. To measure the wavefront we used the averaging of 10 frames from a video camera.

5. Conclusions

We have studied numerically and experimentally wavefront aberrations of the laser light passed through a layer of a turbid medium. It has been shown that centrally symmetric aberrations of both lower and higher orders (defocusing and

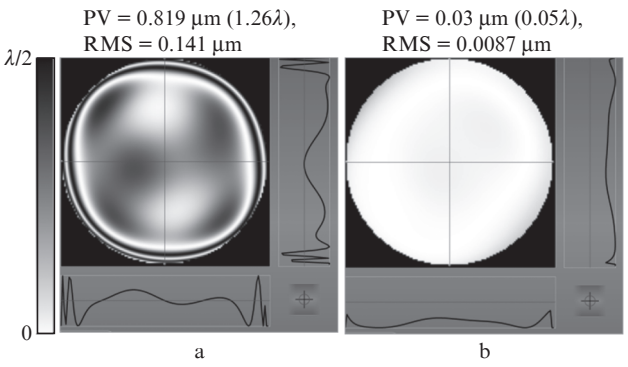

Figure 8. Interferograms and profiles of the wavefront of the light transmitted through a turbid medium at a scattering particle concentration of 7.4×10^5 mm^{-3} (a) before and (b) after correction by the bimorph mirror.

spherical aberration) prevail in the scattered light for a range of scattering particle concentrations from 1.3×10^5 to 10^6 mm^{-3}. Experimentally measured distortions of the wavefront of the light travelled through the suspension of polystyrene microspheres in distilled water has been effectively compensated for by the response functions of the adaptive bimorph mirror with 32 electrodes. The efficiency of correction has amounted to ~95%.

Acknowledgements. The work was supported by the Russian Foundation for Basic Research (Grant No. 16-07-01276a).

References

1. Tuchin V.V. *Lazery i volokonnaya optika v biomeditsinskikh issledovaniyakh* (Lasers and Fibre Optics in Biomedical Research) (Moscow: Fizmatlit, 2010).
2. Mosk A.P., Lagendijk A., Lerosey G., Fink M. *Nat. Photonics*, **6**, 283 (2012).
3. Vellekoop I.M., Mosk A.P. *Opt. Lett*., **32**, 2309 (2007).
4. Bashkatov A.N., Priezzhev A.V., Tuchin V.V. *Kvantovaya Elektron*., **42** (5), 379 (2012) [*Quantum Electron*., **42** (5), 379 (2012)].
5. Vorob'eva E.A., Gurov I.P. *Modeli rasprostraneniya i rasseyaniya opticheskogo izlucheniya v sluchaino neodnorodnykh sredakh* (Models of Propagation and Scattering of Optical Radiation in Randomly Inhomogeneous Media) (Moscow: Meditsina, 2006).
6. Meglinski I.V. *Physiol. Meas*., **23**, 741 (2002).
7. Ramachandran H. *Current Science*, **76**, 1334 (1999).
8. Zhang Y., Chen Y., Yu Y., Xue X., Tuchin V.V., Zhu D. *J. Biomed. Opt*., **18** (7), 077003 (2013).
9. Goodman J.W., Huntley W.H. Jr., Jackson D.W., Lehmann M. *Appl. Phys. Lett*., **8**, 311 (1966).
10. Kogelnik H., Pennington K.S. *J. Opt. Soc. Am*., **58** (2), 273 (1968).
11. Matthews T., Medina M., Maher J., Levinson H., Brown W., Wax A. *Optica*, **1** (2), 105 (2014).
12. Zhou E., Ruan H., Yang Ch., Judkewitz B. *Optica*, **1** (4), 227 (2014).
13. Bertolotti J., van Putten E.G., Blum C., Lagendijk A., Vos W.L., Mosk A.P. *Nature*, **491** (7423), 232 (2012).
14. Vellekoop I.M., Lagendijk A., Mosk A.P. *Nat. Photonics*, **4**, 320 (2010).
15. Katz O., Small E., Silberberg Y. *Nat. Photonics*, **6**, 549 (2012).
16. Conkey D.B., Caravaca-Aguirre A.M., Piestun R. *Opt. Express*, **20**, 1733 (2012).
17. Hsieh C., Pu Y., Grange R., Laporte G., Psaltis D. *Opt. Express*, **18**, 20723 (2010).
18. Popoff S.M., Lerosey G., Carminati R., Fink M., Boccara A.C., Gigan S. *Phys. Rev. Lett*., **104**, 100601 (2010).
19. Hillman T.R., Yamauchi T., Choi W., Dasari R.R., Feld M.S., Park Y., Yaqoob Z. *Scientific Reports*, **3**, 1909 (2013).
20. Kudryashov A.V., Kulakov V.B., Kotsuba Y.V., Novikova L.V., Samarkin V.V. *Proc. SPIE Int. Soc. Opt. Eng*., **3688**, 469 (1999).
21. Bykov A.V., Priezzhev A.V., Myllylä R. *Kvantovaya Elektron*., **41** (6), 557 (2011) [*Quantum Electron*., **41** (6), 557 (2011)].
22. Ma X., Lu J., Brocks S., Jacob K., Yang P., Xin X.-H. *Phys. Med. Biol*., **48**, 4165 (2003).
23. Kirillin M.Yu., Priezzhev A.V. *Kvantovaya Elektron*., **32** (10), 883 (2002) [*Quantum Electron*., **32** (10), 883 (2002)].
24. Wang L., Jacques S. *Computer Programs and Methods in Biomedicine*, **47**, 131 (1995).
25. http://omlc.org/education/ece532/class3/hg.html.
26. Sheldakova J., Cherezova T., Alexandrov A., Rukosuev A.L., Kudryashov A.V. *Proc. SPIE Int. Soc. Opt. Eng*., **5708**, 352 (2005).
27. Aleksandrov A.G., Zavalova V.E., Kudryashov A.V., Rukosuev A.L., Romanov P.N., Samarkin V.V., Sheldakova Yu.V. *Kvantovaya Elektron*., **40** (4), 321 (2010) [*Quantum Electron*., **40** (4), 321 (2010)].
28. Platt B., Shack R. *J. Refractive Surgery*, **17**, 15 (2001).
29. Liang J., Grimm B., Goelz S., Bille J.F. *J. Opt. Soc. Am. A*, **11**, 1949 (1994).
30. Lane R.G., Tallon M. *Appl. Opt*., **31** (32), 6902 (1992).
31. http://www.activeoptics.ru.
32. Galaktionov I.V., Sheldakova Yu.V., Kudryashov A.V. *Kvantovaya Elektron*., **45** (2), 143 (2015) [*Quantum Electron*., **45** (2), 143 (2015)].
33. Wyant J.C., Creath K., in *Proceedings of Applied Optics and Optical Engineering* (San Diego: Academic Press, 1992) pp 27–39.
34. Samarkin V., Aleksandrov A., Kudryashov A. *Proc. SPIE Int. Soc. Opt. Eng*., **4493**, 269 (2002).
35. Samarkin V., Kudryashov A. *Proc. SPIE Int. Soc. Opt. Eng*., **7789**, 77890B (2010).
36. Rukosuev A., Alexandrov A., Zavalova V., Samarkin V., Kudryashov A. *Proc. SPIE Int. Soc. Opt. Eng*., **4493**, 261 (2002).